Available online at www.sciencedirect.com
SCIENCE DIRECT®
Applied Catalysis A: General 260 (2004) 215–222
APPLIED CATALYSIS A: GENERAL
www.elsevier.com/locate/apcata

Preparation and photocatalytic properties of a nanometer ZnO–SnO_2 coupled oxide

Maolin Zhang, Taicheng An*, Xiaohong Hu, Cun Wang, Guoying Sheng, Jiamo Fu

State Key Laboratory of Organic Geochemistry, Guangdong Key Laboratory of Environmental Resources Utilization and Protection, Guangzhou Institute of Geochemistry, Chinese Academy of Sciences, Guangzhou 510640, PR China

Received in revised form 27 September 2003; accepted 18 October 2003

Abstract

A nanometer coupled oxide ZnO–SnO_2 was prepared using the co-precipitation method employing $NH_3{\cdot}H_2O$ as the precipitant. The oxide was characterized by X-ray diffraction (XRD), transmission electron microscope (TEM) and UV diffuse reflectance spectrum (DRS). The photocatalytic activity of nanometer coupled oxides was studied using methyl orange as a mode organic pollutant. The relationship between the photocatalytic activity and the microstructure of nanometer coupled oxides was also discussed in the paper. Experimental results showed that the nanometer coupled oxides mainly consist of nanometer ZnO and SnO_2, and they have the same excellent photocatalytic activity as Degussa P25 TiO_2 for the degradation of methyl orange (MO). Moreover, the photocatalytic activity of the coupled oxides increases gently at first, then decreases rapidly with the increase of the calcination temperature. But a small amount of nanometer Zn_2SnO_4 was formed in the mixture of coupled oxides when the calcination temperature was higher than 700 °C.

Keywords: Coupled oxides; Nanometer photocatalyst; Co-precipitation method; Photocatalytic degradation; Organic pollutants

1. Introduction

Since Frank and Bard conducted photocatalytic degradation of CN^- in aqueous solutions firstly [1], heterogeneous photocatalysis has received increasing attention over two decades for purifying a great variety of environmental pollutants in water and air [2–5]. However, the development of a practical water treatment system relative to the photocatalytic oxidation has not yet been successfully achieved. The high degree of recombination of photogenerated electrons and holes is a major limiting factor controlling its photocatalytic efficiency and impeding the practical application of this technique in the degradation of contaminants in water and air. Thus, a major challenge in heterogeneous photocatalysis is the need to increase the charge separation efficiency of the photocatalyst. Coupled semiconductor photocatalysts exhibit a very high photocatalytic activity for both gas- and liquid-phase reactions by increasing the charge separation and extending the energy range of photoexcitation. At the same time, their physical and optical properties are greatly modified [6]. In the past several years, the researchers had much interest in coupling two semiconductor particles with difference band-gap widths, and many research groups have carried out the photocatalytic activity experiments of various coupled semiconductor particle systems, such as TiO_2–SnO_2 [6–10], TiO_2–WO_3 [11–15], TiO_2–MoO_3 [13], TiO_2–CdS [16,17], CdS–ZnO [17], CdS–AgI [18], ZnO–ZnS [19], TiO_2–ZrO_2 [20], TiO_2–Fe_2O_3 [21,22]. However, the photocatalytic activity of coupled oxides ZnO–SnO_2 is little reported [23]. In our previous study [24], a nanometer coupled oxide ZnO–SnO_2 was prepared and its photocatalytic activities were evaluated using MO as a model organic compound. But the preparation method is very time consuming for completely eliminating the chloride and sulfate, which can embed into the fresh prepared photocatalyst.

In the present paper, a nanometer coupled oxide ZnO–SnO_2 was also prepared for the purpose of saving time, convenient operation and improving photocatalytic efficiency with a simplified co-precipitation method by employing $NH_3{\cdot}H_2O$ as the precipitant. Its photocatalytic activities were also evaluated using methyl orange as a model organic compound. In the process, the chloride ion and sulfate ion can exist as the salts of NH_4Cl and $(NH_4)_2SO_4$, and

* Corresponding author. Tel.: +86-20-85291501; fax: +86-20-85290706.
E-mail address: antc99@gig.ac.cn (T. An).

0926-860X/$ – see front matter © 2003 Elsevier B.V. All rights reserved.
doi:10.1016/j.apcata.2003.10.025

these salts can be easily eliminated from the photocatalyst in the post-calcination procedure. The factors affecting the photocatalytic activity, such as the heat-treating temperature for ZnO–SnO_2 and the concentrations of NaCl, Na_2SO_4 and KNO_3 in the suspension, have also been examined. It was found that the coupled semiconductor photocatalyst ZnO–SnO_2 has better photocatalytic activity than that of single semiconductor photocatalyst ZnO or SnO_2. Moreover, the nanometer coupled oxide ZnO–SnO_2 prepared by using $NH_3{\cdot}H_2O$ as the precipitant has smaller size and better photocatalytic activities than that of the coupled oxides prepared by using NaOH as the precipitant under the identical conditions.

2. Experimental

2.1. Material and apparatus

The reagents ($SnCl_4{\cdot}5H_2O$, $ZnSO_4{\cdot}7H_2O$, $NH_3{\cdot}H_2O$, MO) are all analytic reagent grade. The photocatalytic reactions take place in a 100 ml Pyrex glass bottle under irradiation of a 300 W high pressure Hg lamp (GGZ300, Shanghai Yaming Lighting Co., Ltd) with a maximum emission at about 365 nm. The MO concentration was analyzed by UV-Vis spectroscopy (Thermo Spectronic/Heλios α) at its maximum absorption wavelength of 464 nm. A Rigaka D/max-1200 diffractometer with Cu Kα radiation ($\lambda = 0.15418$ nm), the accelerating voltage of 40 kV, emission current of 30 mA and the scanning speed of 4°/min was used to determine the crystal phase composition of the coupled oxides prepared at room temperature. And a transmission electron microscope (Jeol JEM-100CX II TEM) was used to observe the shape and size of the prepared photocatalysts. A CARY 100 spectrophotometer was used to carry out the UV-Vis diffuse reflectance spectroscopy, and the $BaSO_4$ high reflectance white optical paint was used as a reference material.

2.2. Preparation for nanometer photocatalyst

Nanometer coupled oxide ZnO–SnO_2 was prepared using the co-precipitation method. $SnCl_4{\cdot}5H_2O$ and $ZnSO_4{\cdot}7H_2O$ were used as the starting materials and $NH_3{\cdot}H_2O$ as the precipitant without further purification. $SnCl_4{\cdot}5H_2O$ and $ZnSO_4{\cdot}7H_2O$ in a molar ratio of 2:1 were dissolved in a minimum amount of deionized water, The 1:1 (v/v) NH_3 aqueous solution was added dropwise to the vigorously stirred mixed solution; then the pH value of the solution was adjusted to about 7 and a large amount of white slurry was formed. The resulting slurry was continuously stirred for 12 h, then filtered without further washing, and finally dried in air at about 100 °C to obtain the precursor of ZnO–SnO_2 photocatalyst. Besides the ZnO–SnO_2, as its reference, the nanometer ZnO and SnO_2 were also prepared by the same procedure as mentioned above except that the starting material is $SnCl_4{\cdot}5H_2O$ for SnO_2 and $ZnSO_4{\cdot}7H_2O$ for ZnO, respectively.

2.3. Photocatalytic procedure

Photocatalytic experiments were conducted to photocatalytically degrade MO in water. The MO is used without further purification, and the initial concentration was prepared to be 20 mg l^{-1}. The photocatalytic reactor consists of two parts: a 100 ml Pyrex glass bottle and a 300 W high pressure Hg lamp that was parallel to the Pyrex glass bottle. In all experiments, the reaction temperature was kept at 25 ± 2 °C by using an air-conditioner. Reaction suspensions were prepared by adding 0.25 g of photocatalyst powders into 100 ml MO aqueous solutions. Prior to irradiation, the suspension was sonicated for 15 min and then stirred in a dark for 30 min to establish adsorption–desorption equilibrium. The suspension containing MO and photocatalyst were then irradiated under the UV light, and the photocatalytic reaction timing was started.

At given time intervals, analytical samples were taken from the reaction suspension, centrifuged at 9000 rpm for 10 min, and filtered through a 0.2 μm millipore filter. Then the filtrate was analyzed.

3. Results and discussion

3.1. Characterization of nanometer coupled oxide photocatalyst

The XRD patterns of the coupled oxide powders calcined at different temperatures are shown in Fig. 1. The phases of the photocatalysts are the couple of ZnO and SnO_2, but the Zn_2SnO_4 phase emerges at 700 °C.The diffraction peaks are continuously getting sharper with increasing calcination temperature, which reveals that the grain size become larger with increasing calcination temperature. The mean size of ZnO or SnO_2 both in the single oxide and the coupled oxide ZnO–SnO_2, calcined at 300, 350, 400, 500, 700, and 900 °C for 2 h, respectively, can be calculated by the

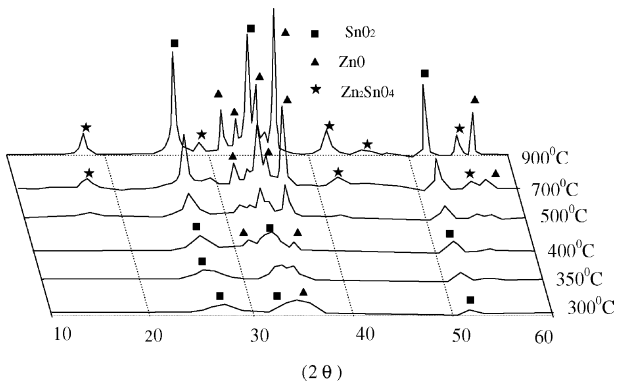

Fig. 1. The XRD patterns of ZnO–SnO_2 calcined at different temperatures.

Table 1
The dependence of mean crystallite size on different heat-treating conditions

Mean size (nm)	Calcination temperature (°C)					
	300	350	400	500	700	900
Coupled oxides						
ZnO	1.7	2.1	8.3	13.2	45.4	95.9
SnO_2	0.8	1.2	3.3	8.2	19.1	50.8
Zn_2SnO_4					3.4	13.6
Single oxides						
ZnO	4.7	9.3	25.2	50.0	102.6	221.5
SnO_2	1.3	2.1	4.7	10.5	20.5	59.4

Scherrer formula [25], and the phases and the mean size are listed in Table 1. Table 1 shows that the mean size of ZnO and SnO_2 become larger and larger both in the single and coupled oxides when the calcination temperature increased from 300 to 900 °C. It is also noted that in coupled oxides, the mean size of both oxides and Zn_2SnO_4 are significantly smaller when using $NH_3{\cdot}H_2O$ as the precipitant than when using NaOH as the precipitant under the identical calcination temperature. Especially, the growth of Zn_2SnO_4 is slow, and ZnO and SnO_2 in the coupled oxide powders do not disappear at the calcination temperature of 900 °C, which disagrees with the previous results [24]. It is reported that the ZnO always has larger grain size than SnO_2 at the same calcination temperature [26], and that the growth of ZnO crystallites was greatly restrained by the presence of SnO_2 [27,28]. The same results were also obtained here. Compared with the results in Table 1, we can conclude that the mean size of both ZnO and SnO_2 are larger in the single oxides than those of in the coupled oxides. In addition, in the coupled oxides, the existence of NH_3 and (or) NH_4^+ in the precursor may prevent ZnO from densification and the formation of Zn_2SnO_4, and thus, the mean size of ZnO and Zn_2SnO_4 in the coupled oxide powder calcined at 900 °C are just about 95.9 and 13.6 nm, respectively, which are much smaller than that reported in previous study [24].

The TEM photographs of the coupled oxide powders calcined at 350, 500, 700, and 900 °C are given in Fig. 2. The TEM photographs show that coupled oxide powder is of an equable distribution except for a little aggregated particulate, and have the shape of short-pillared crystallites. On the other hand, the TEM photographs show that coupled oxide powder is nanometer scale, which is in reasonable agreement with the results obtained from the XRD. Moreover, it is also easy to see from the TEM photographs that the mean size of coupled oxides particle increases significantly with increase of the calcination temperature. For example, the mean size of ZnO and SnO_2 in the coupled oxides calcined at 350 °C are about 2.2 and 1.2 nm, respectively, while the

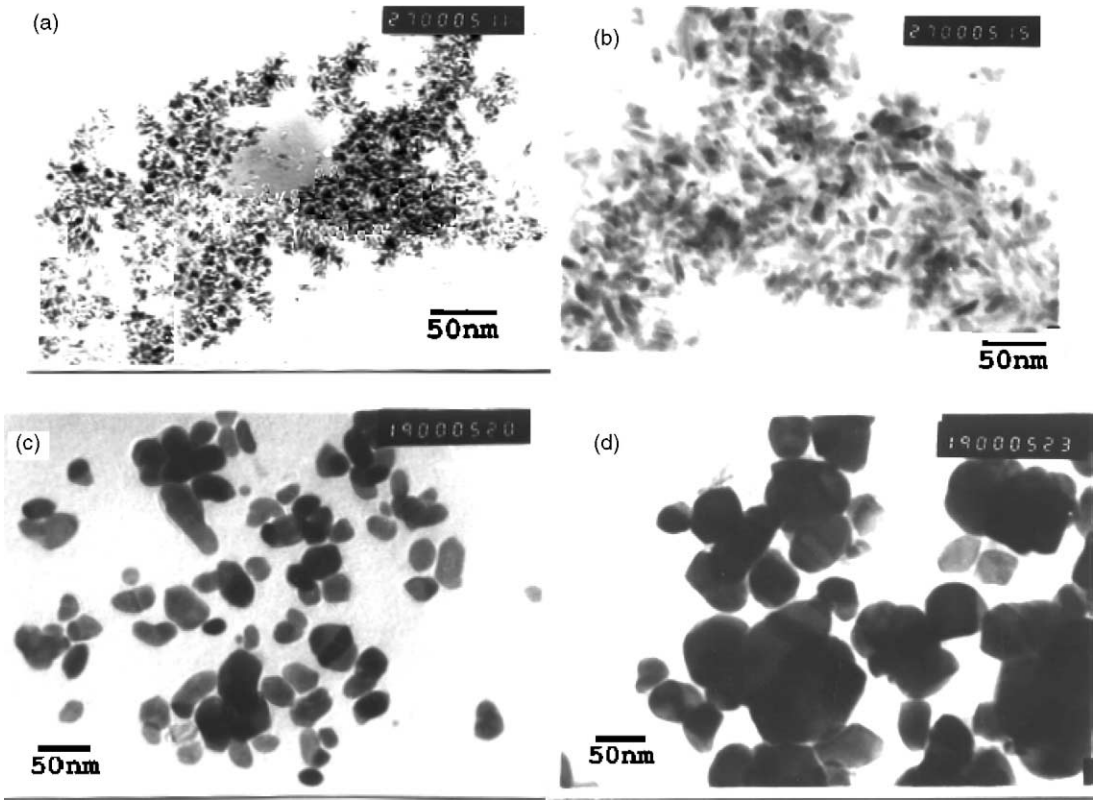

Fig. 2. The TEM photographs of ZnO–SnO_2 calcined at different temperatures (a) 350 °C, (b) 500 °C, (c) 700 °C, (d) 900 °C.

mean size of ZnO and SnO_2 in the coupled oxides calcined at 900 °C are about 95.9 and 50.8 nm, respectively.

The diffuse reflectance spectroscopy (DRS) and its applications to study metal oxides have been reviewed recently [29]. In a diffuse reflectance spectrum, the ratio of the light scattered from a thick layer of sample and that from an ideal non-absorbing reference sample is measured as a function of the wavelength. The UV-Vis diffuse reflectance spectra of ZnO–SnO_2 calcined at 350, 500, 700, 900 °C, respectively, are given in Fig. 3, where the scale labeled "absorbance" are the negative logarithm value of the experimentally determined diffuse reflectance of samples. From the figure we can find that in the UV region between 200 and 400 nm, several absorption bands are observed at each curve. The DRS of ZnO–SnO_2 calcined at 350 °C gives two absorption peaks at 208.7 and 259.5 nm with an absorption edge at 360.3 nm. The two absorption peaks are expected for the interband transitions of nanometer SnO_2 and ZnO, respectively. It is to be noted that both absorption peaks in the DRS of ZnO–SnO_2 are red-shifted from 208.7 and 259.5 nm to 211.6 and 273.7 nm, and by increasing the calcination temperature from 350 to 900 °C, the shifting number became 2.9 and 14.2 nm, respectively. Such shifts may be attributed to the changes of crystallite phase and size of coupled oxides, defects, and so on. But the shift of the former absorption peak is less than that of the later. In addition to the red shift, a weak band at 374.1 nm is also observed in the DRS of ZnO–SnO_2 calcined at 800 and 900 °C, which seems to be related to little Zn_2SnO_4 crystallites. At the same time, it is also found that the UV absorption edge wavelength in the DRS of ZnO–SnO_2 increases with increasing the calcination temperature. According to the literature [30], the absorption edge wavelengths of ZnO–SnO_2 calcined at 350, 500, 700, and 900 °C are determined to be 360.3, 376.6, 391.1, and 405.4 nm corresponding to the band gap energies of 3.44, 3.29, 3.17, 3.06 eV, respectively. The absorption edge wavelength and the band gap energies of ZnO–SnO_2 calcined at different temperatures are listed in Table 2. The band gap energies of materials are related to the photocatalytic activity of materials for the degradation of pollutants. The larger the band gap energy of a material is, the greater the redox potential of the photogenerated electron-hole pairs is. Thus, these exhibit more redox capacity. As is proved by the following photocatalytic activity experiment of ZnO–SnO_2 for the degradation of MO, the greater the band gap energy of ZnO–SnO_2 is, the greater the photocatalytic activity is for degradation of organic pollutants.

Table 2
Absorption edges and band gap energy of couple oxides calcinated at different temperatures

Calcination temperature (°C)	Absorption edge (nm)	Band gap energy (eV)
350	360.3	3.44
500	376.6	3.29
700	391.1	3.17
900	405.4	3.06

3.2. Photocatalytic activity of the nanometer coupled oxides

3.2.1. Degradation kinetics of MO

The time-dependent UV-Vis spectra of MO during the irradiation are illustrated in Fig. 4. It can be seen that the maximum absorbance of 464 nm disappears completely after irradiation for 30 min. In addition to experiments with ZnO–SnO_2 and irradiation, both blank experiments were investigated in the absence of irradiation with ZnO–SnO_2

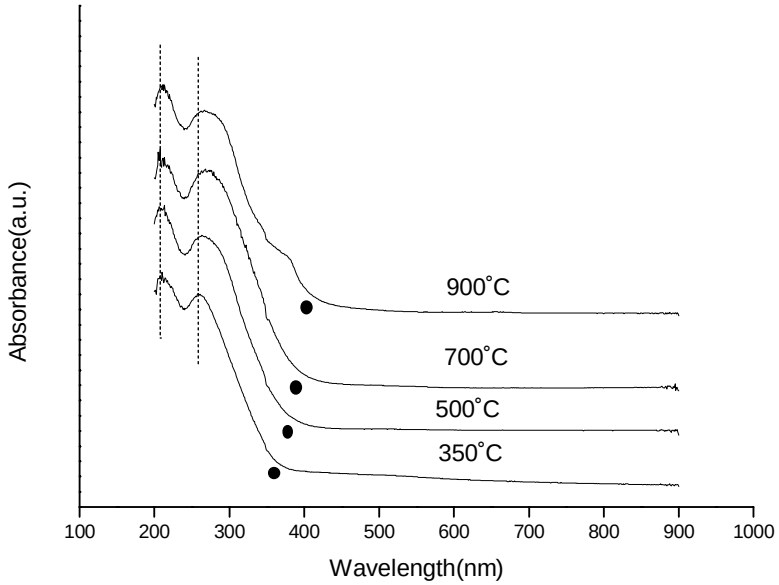

Fig. 3. The UV-Vis diffuse reflectance spectra of ZnO–SnO_2 calcined at different temperatures.

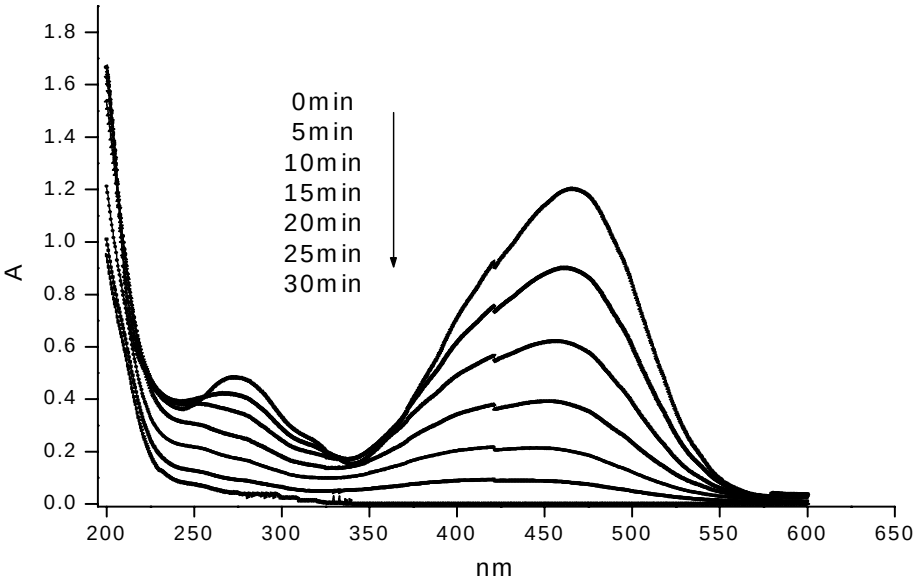

Fig. 4. The absorbance spectra changes of MO solution in the presence of ZnO–SnO_2 and irradiation.

or in the presence of irradiation without ZnO–SnO_2. Results show that MO cannot be degraded under the present experimental conditions. However, in the presence of irradiation and ZnO–SnO_2, MO can easily be photocatalytically degraded, and the result is shown in Fig. 5. For the purposes of comparison, the photocatalytic degradation of MO was carried out using various photocatalysts, Degussa P25 TiO_2, ZnO–SnO_2 prepared by using NaOH as the precipitant (denoted as ZnO–SnO_2/NaOH), SnO_2 alone or ZnO alone. These results are also shown in Fig. 5. These experimental results show that the Coupled oxide ZnO–SnO_2 has greatly higher photocatalytic efficiency than ZnO or SnO_2 alone. At the same time, ZnO–SnO_2 has better photocatalytic activities than ZnO–SnO_2/NaOH, and exhibits almost the same excellent photocatalytic activity as Degussa P25 TiO_2. Moreover, under present experimental conditions, the degradation reactions of MO are all the first-order reactions during the first 15 min of irradiation, and the apparent rate constants for ZnO–SnO_2, Degussa P25 TiO_2, ZnO–SnO_2/NaOH, ZnO and SnO_2 are 0.0865, 0.0822, 0.0339, 0.0335, 0.0124 min^{-1}, respectively. It is easily seen that the degradation rate of MO using ZnO–SnO_2 as a photocatalyst is faster than that using SnO_2, ZnO, ZnO–SnO_2/NaOH or Degussa P25 TiO_2 as a photocatalyst by 597.5, 158.2, 155.2, and 5.2%, respectively.

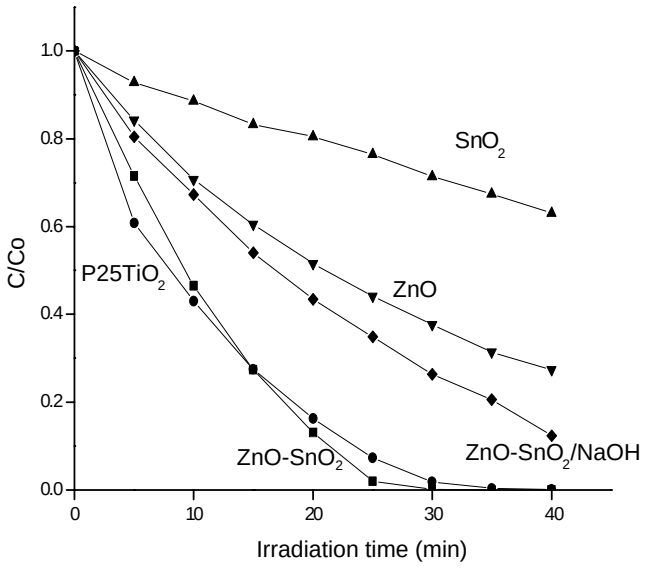

Fig. 5. The photocatalytic activity of different photocatalysts calcined at 350 °C for 2 h (ZnO–SnO_2/NaOH calcined at 600 °C for 10 h).

The heterogeneous photocatalysis may be pH dependent, and the decomposition of MO may depend on the pH of reaction solution. The dependence of the pH value of solution on the degradation rate of MO was investigated in detail in our previous study [24], the result showed that the degradation rate of MO decreased with increasing the initial pH value of reaction suspensions, however, the degradation rate of MO decreased slightly when the initial pH value of reaction suspensions was increased from 4.22 to 7.12. In the present paper, the initial pH value of reaction suspensions containing different photocatalysts was also measured. Results show that the initial pH values of reaction suspensions containing ZnO–SnO_2, ZnO–SnO_2/NaOH, Degussa P25 TiO_2, ZnO alone and SnO_2 alone are 7.09, 7.12, 6.37, 7.15, and 6.17, respectively. It is noted that though the initial pH values of reaction suspensions of SnO_2 or Degussa P25 TiO_2 are lower, the initial pH values all are near 7. Since the differences in the degradation rate of MO from the initial pH values of reaction suspensions are very small at this tested range, the effect of the initial pH values of reaction suspensions containing tested photocatalysts on the degradation rate of MO can be ignore in the present study.

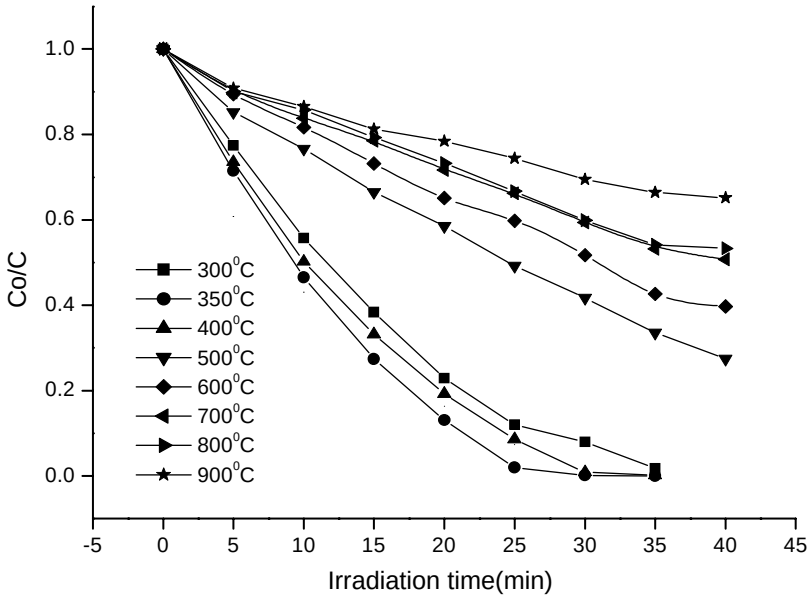

Fig. 6. The effect of calcination temperature on the photocatalytic activity of ZnO–SnO_2.

Therefore, the differences in the degradation rate of MO are mainly attributed to the different photocatalytic activity of various photocatalysts.

3.2.2. Effect of calcination temperature on the photocatalytic activity

The effect of heat-treating temperature on the photocatalytic activity of ZnO–SnO_2 is shown in Fig. 6. The degradation rate of MO is decreased with increasing calcination temperature except for 300 °C, which may be attributed to some variation in phase composition and in particle size. For samples calcined at 300, 350, or 400 °C, the size of ZnO and SnO_2 in coupled oxides are 1.7, 2.1, or 8.3 nm and 1.8, 1.2, or 3.3 nm, respectively. The high photocatalytic activity of ZnO–SnO_2 was obtained at lower calcination temperature, which was attributed to quantum size effects. The dimension particles show quantum size effects and exhibit high photocatalytic efficiency. But the photocatalytic activity of ZnO–SnO_2 calcined at 300 °C is slightly lower than that of the photocatalyst calcined 350 °C, which may be due to the partial formation of crystallite oxides. With increasing calcination temperature, the size of crystallite oxides increases, which is supported by XRD and TEM photography, resulting in a reduction in quantum size effects. At the same time, when temperature is higher than 700 °C, oxides of both ZnO and SnO_2 partly transform to Zn_2SnO_4 poor photocatalyst [31], resulting in a significant reduction in the photocatalytic activity of coupled oxides.

3.2.3. Effect of anion ions on the photocatalytic activity

In real wastewater and natural water, anion ions are frequently present. Many systematic studies [32–37] have also been conducted to elucidate the effect of anions, such as SO_4^{2-}, NO_3^-, Cl^-, ClO_4^-, and CO_3^{2-}, on the photocatalytic activity of TiO_2 towards certain organic substrates. The effect of several anions, such as SO_4^{2-}, NO_3^-, and Cl^-, on the photocatalytic activity of coupled oxides was also studied here. Fig. 7 shows the dependence of the changes of the ratios of the residual MO concentrations to its initial ones on the reaction time, illustrating the effect of Cl^-, NO_3^- and SO_4^{2-} on the photocatalytic degradation of MO under the natural pH value. As Fig. 7 shows, NO_3^- has little effect on the photocatalytic activity, which agrees with the literature [33,34], while other tested anions show an inhibitive effect on the photocatalytic reaction of MO. Such influence is enhanced with the increase in anion concentration. A plausible reason for the phenomenon may be that the Cl^- ions act as a radical scavenger, and can react with hydroxyl radical to form $^{\bullet}Cl_2^-$ or $^{\bullet}ClOH^-$ [38,39], which may retard the photocatalytic oxidation reaction dramatically. But the inhibitive effect of SO_4^{2-} ion can be attributed to the competition adsorption between SO_4^{2-} and MO at the photocatalyst surface.

3.3. Photocatalytic reaction mechanism

According to the mechanism of semiconductor photocatalysis, on irradiation of a photocatalyst particle with supraband gap light, photogenerated electron-hole pairs are formed, and there is a finite possibility that the electron and hole will overcome their mutual electrostatic attraction and become spatially separated. These will then diffuse to the surface, where the electron will be captured by O_2 and the hole by adsorbed hydroxide to form $^{\bullet}OH$ radicals. However, the distance that the holes move in a field-free region before recombination with an electron is about 0.1 μM. Before the electrons and holes reach the surface, there is a significant chance of recombination, and this is an important

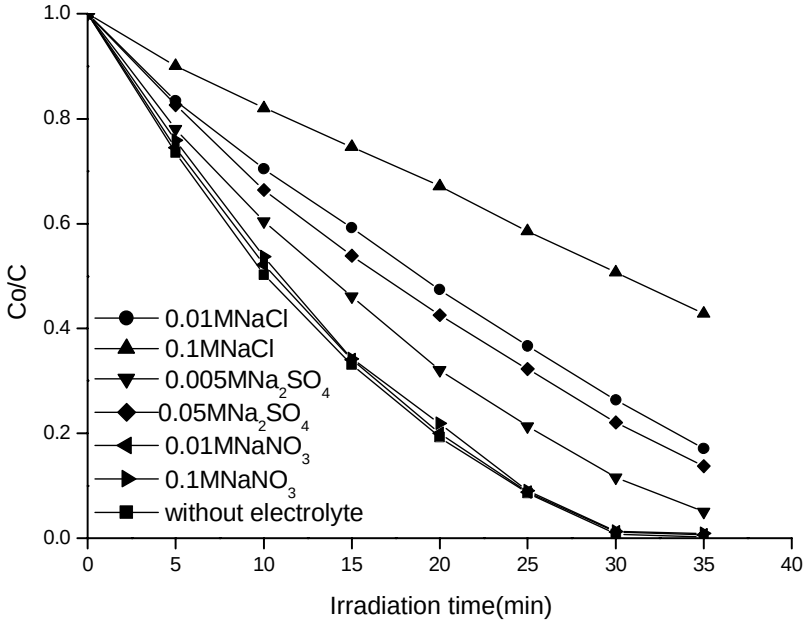

Fig. 7. The effect of various anions on the photocatalytic degradation of MO.

source of inefficiency in systems employing semiconductor catalysts for photochemical conversion of light [40]. But semiconductor nanocrystallites exhibit interesting photocatalytic properties differing significantly from those observed for the related bulk material. A reduction in particle size to the nanometer scale results in quantum size effects at dimensions comparable to the Bohr-diameter of the exciton. At such crystallite dimensions, the photogenerated electron-hole-pairs are spatially confined if the diameter of the crystallites is smaller than the Bohr-diameter of the exciton [41]. In the present experiment, in the coupled oxides, the particle size of prepared coupled oxides are just 2.1 and 1.2 nm for ZnO and SnO_2 calcined at 350 °C, respectively. Thus, this nanometer coupled oxide has a good quantum size effect, and exhibit high photocatalytic efficiency.

On the other hand, the conduction band (CB) position of SnO_2 is lower than that of ZnO, so that the former can act as a sink for the photogenerated electrons in the coupled oxides [10,23,37]. Since the holes move in the opposite direction from the electrons, the photogenerated holes in SnO_2 might be trapped within the ZnO particle, making charge separation more efficient; then the recombination of electrons and holes in ZnO–SnO_2 is greatly suppressed. A mechanistic scheme of the charge separation and photocatalytic reaction for ZnO–SnO_2 photocatalyst is shown in Fig. 8. This is another reason that the nanometer coupled oxide ZnO–SnO_2 possessed both higher photocatalytic oxidation and reduction activities than those of single ZnO or SnO_2.

From above mentioned, a high photocatalytic activity in the coupled oxides may be attributed to the quantum size effect of nano scale particles and the charge separation in the coupled oxide. It can be see from Table 1, the mean size of ZnO or SnO_2 both in the single and the coupled oxide calcined 350 °C were all below 10 nm, and the difference in mean size of ZnO or SnO_2 was very small. However, the difference in the photocatalytic activity of single oxide and coupled oxide was much larger. Thus, we may conclude that the separation of the photogenerated electrons and holes play

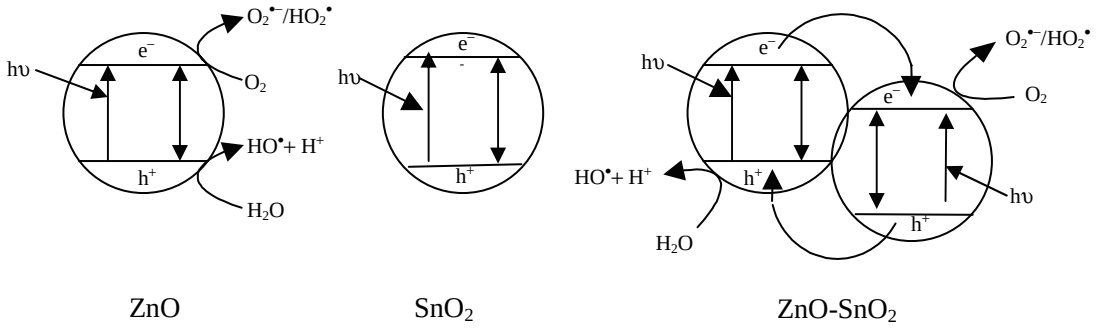

Fig. 8. A schematic diagram illustrating the principle of charge separation and photocatalytic activity for the couple oxides.

an important role in the photocatalytic activity enhancement in the coupled oxides.

4. Conclusions

The following conclusions can be drawn from the present study: (1) The mean size of prepared coupled oxides is of namemeter scale,and the coupled oxides have a better photocatalytic activity than that of either of the single semiconductor photocatalysts, ZnO or SnO_2. (2) The nanometer coupled oxide ZnO–SnO_2 prepared by employing $NH_3{\cdot}H_2O$ as the precipitant has smaller size and better photocatalytic activities than those of the coupled oxides prepared by using NaOH as the precipitant under the identical conditions. (3) The heat-treating temperature greatly affected the photocatalytic activity of coupled oxides ZnO–SnO_2. The higher the calcination temperature, the larger the mean size of nanometer coupled oxides, and the better the photocatalytic activity of ZnO–SnO_2 for MO degradation.

Acknowledgements

The authors thank the editor for his English corrections and the anonymous reviewers for their valuable comments on the manuscript. And the authors also appreciate the assistance from professor Guangxin Wang. Financial support from National Nature Science Foundation of China (No. 40302013), Tenth Fifth-year Project of Guangdong province, China (No. 2001A3040101), and Nature Science Foundation of Guangdong province, China (No. 030466) is gratefully acknowledged.

References

[1] S.N. Frank, A.J. Bard, J. Am. Chem. Soc. 99 (1977) 303.
[2] D.F. Ollis, Environ. Sci. Technol. 19 (1985) 480.
[3] C. Kormann, D.W. Bahnemann, M.R. Hoffmann, Environ. Sci. Technol. 25 (1991) 494.
[4] M.R. Hoffmann, S.T. Martin, W. Choi, D.W. Bahnemann, Chem. Rev. 95 (1995) 69.
[5] J. Peral, D.F. Ollis, J. Catal. 136 (1992) 554.
[6] X.Z. Li, F.B. Li, C.L. Yang, W.K. Ge, J. Photochem. Photobiol. A: Chem. 141 (2001) 209.
[7] I. Bedja, P.V. Kamat, J. Phys. Chem. 99 (1995) 9182.
[8] K. Vinodgopal, I. Bedja, P.V. Kamat, Chem. Mater. 8 (1996) 2180.
[9] J. Lin, J.C. Yu, D. Lo, S.K. Lam, J. Catal. 183 (1999) 368.
[10] K. Vinodgopal, P.V. Kamat, Environ. Sci. Technol. 29 (1995) 841.
[11] L.Y. Shi, C.Z. Li, H.C. Gu, D.Y. Fang, Mater. Chem. Phys. 62 (2000) 62.
[12] Y.R. Do, W. Lee, K. Dwight, A. Wold, J. Solid State Chem. 108 (1994) 198.
[13] K.Y. Song, M.K. Park, Y.T. Kwon, H.W. Lee, W.J. Chung, W.I. Lee, Chem. Mater. 13 (2001) 2349.
[14] T. Ohno, F. Tanigawa, K. Fujihara, S. Izumi, M. Matsumura, J. Photochem. Photobiol. A: Chem. 118 (1998) 41.
[15] Y.T. Kwon, K.Y. Song, W.I. Lee, G.J. Choi, Y.R. Do, J. Catal. 191 (2000) 192.
[16] R. Vogel, P. Hoyer, H. Weller, J. Phys. Chem. 98 (1994) 3183.
[17] L. Spanhel, H. Weller, A. Henglein, J. Am. Chem. Soc. 109 (1987) 6632.
[18] K.R. Gopidas, M. Bohorquez, P.V. Kamat, J. Phys. Chem. 94 (1990) 6435.
[19] J. Rabani, J. Phys. Chem. 93 (1989) 7707.
[20] J.C. Yu, J. Lin, R.W.M. Kwok, J. Phys. Chem. B 102 (1998) 5094.
[21] B. Pal, M. Sharon, G. Nogami, Mater. Chem. Phys. 59 (1999) 254.
[22] B. Pal, T. Hata, K. Goto, G. Nogami, J. Mol. Catal. A: Chem. 169 (2001) 147.
[23] K. Tennakone, J. Bandara, Appl. Catal. A: Gen. 208 (2001) 335.
[24] C. Wang, J.C. Zhao, X.M. Wang, B.X. Mai, G.Y. Sheng, P.A. Peng, J.M. Fu, Appl. Catal. B: Environ. 39 (2002) 269.
[25] H.P. Klug, L.E. Alexander, X-Ray Diffraction Procedures for Polycrystalline and Amorphous Materials, Wiley, New York, 1974, p. 618.
[26] J.H. Yu, G.M. Choi, Sens. Actuators B 61 (1999) 59.
[27] N. Daneu, A. Recnik, S. Bernik, D. Kolar, J. Am. Ceram. Soc. 83 (2000) 3165.
[28] J.H. Yu, G.M. Choi, Sens. Actuators B 52 (1998) 251.
[29] B.M. Weckhuysen, R.A. Sehoonheydt, Catal. Today 49 (1999) 441.
[30] P.L. Provenzano, G.R. Jindal, J.R. Sweet, W.B. White, J. Luminesc. 92 (2001) 297.
[31] C. Wang, X.M. Wang, J.C. Zhao, B.X. Mai, G.Y. Sheng, P.A. Peng, J.M. Fu, J. Mater. Sci. 37 (2002) 1.
[32] D.W. Chen, A.K. Ray, Water Res. 32 (1998) 3223.
[33] K.H. Wang, Y.H. Hsieh, M.Y. Chou, C.Y. Chang, Appl. Catal. B: Environ. 21 (1999) 1.
[34] W.H. Leng, H. Liu, S.A. Cheng, J.Q. Zhang, C.N. Chao, J. Photochem. Photobiol. A: Chem. 131 (2000) 125.
[35] I. Arslan, I.A. Balcioglu, D.W. Bahnemann, Appl. Catal. B: Environ. 26 (2000) 193.
[36] A. Piscopo, D. Robert, J.V. Weber, Appl. Catal. B: Environ. 35 (2001) 117.
[37] M. Abdullah, G.K.-C. Low, R.W. Matthews, J. Phys. Chem. 94 (1990) 6820.
[38] V. Nadtochenko, J. Kiwi, Environ. Sci. Technol. 32 (1998) 3273.
[39] V. Nadtochenko, J. Kiwi, Environ. Sci. Technol. 32 (1998) 3282.
[40] H. Gerischer, Electrochim. Acta 38 (1993) 3.
[41] Y. Wang, N. Herron, J. Phys. Chem. 95 (1991) 525.